Selectable Synthesis of 2-D MoS_2 and Its Electronic Devices: From Isolated Triangular Islands to Large-Area Continuous Thin Film

Wai Ching Cho, Kam Lam Wu, Pak San Yip, Xinsheng Wang, Yang Chai, *Senior Member, IEEE*, and Kei May Lau, *Fellow, IEEE*

***Abstract*—We report on the controllable and selectable synthesis of two-dimensional (2-D) molybdenum disulfide (MoS_2) by molybdenum trioxide sulfurization with chemical vapor deposition. By controlling the sulfurization timing and substrates positions, the selectable growth of MoS_2 isolated triangular islands and continuous thin film was successfully performed independently with the same home-built furnace setup. Also, we found that the hydrofluoric acid substrate treatment took effects on MoS_2 nucleation seed densities and modulated the sizes of the triangular islands. Atomic force microscopy and Raman and photoluminescence spectroscopy were used to characterize and compare the properties of MoS_2 triangular islands and continuous thin film. The MoS_2 triangular islands were monolayers and highly crystalline in nature; where the continuous thin film was formed by small grain size MoS_2 nanosheets with smooth surface morphology and a large covered area of up to centimeters. Back-gated field effect transistors (FETs) of as-grown MoS_2 triangular islands and continuous thin film were fabricated to analyze their electrical properties. The electron mobilities were measured to be 11.42 and 4.04 $cm^2/V{\cdot}s$ respectively, and with an excellent on/off current ratio up to over 10^8, which demonstrated the good quality of the as-grown MoS_2 samples. Furthermore, both the MoS_2 triangular islands and continuous thin film FETs exhibited a near ideal current saturation characteristic, which shows the real potential of future applications for 2-D electronic devices.**

***Index Terms*—2D materials, MoS_2, MoO_3, chemical vapor deposition, field effect transistor.**

I. Introduction

MOLYBDENUM disulfide (MoS_2), a representative of two dimensional (2D) layered materials, is regarded as one of the attractive candidates to supplement silicon for future logic devices and circuits. With its layer dependent properties and existence of a semiconductor band gap [1]–[4], MoS_2 shows the potential to be the building block for future logic applications beyond graphene. Exfoliated monolayer MoS_2 field effect transistors (FETs) have been demonstrated with an excellent mobility of 217 $cm^2/V.s$, on/off ratio up to 10^8 and good immunity to the short channel effect [3]. In manufacturing, micro-mechanical exfoliation is not a reliable fabrication method as the size and thickness of the produced MoS_2 flakes are uncontrollable. Chemical vapor deposition (CVD) has been demonstrated as the most promising synthesis method in recent studies [5]–[20], with reasonable electrical performance compared to that of natural MoS_2 crystals. The most common method of MoS_2 CVD synthesis is the sulfurization of solid molybdenum trioxide (MoO_3). The main outcomes are either disconnected triangular islands [5]–[11] or large area continuous films [14]–[19]. Thanks to their highly crystalline nature, back-gated devices with SiO_2 gate dielectric based on as-grown mono- and bilayer MoS_2 triangular islands yield comparable field effect mobilites of up to $\sim$10 $cm^2/V.s$ [36] and $\sim$17 $cm^2/V.s$ [7] respectively, with an on/off current ratio of up to $\sim 10^8$ at room temperature. The reported continuous films are mainly formed by polycrystalline mono- to few layer MoS_2 grains, and yield lower field effect mobilites with a range of 0.003 to 7.23 $cm^2/V.s$ and an on/off current ratio of up to $\sim 10^6$ [15]–[19]. Although the MoS_2 continuous films have a poorer electrical performance compared to triangular islands, their continuity in nature and large area coverage have advantages in the real manufacturing process. Understanding the growth mechanisms of 2D materials is important to achieve the ultimate goal, wafer-scale synthesis with high electrical performance. However, there has been an absence of clear mechanisms and critical parameters to differentiate between the CVD synthesis of MoS_2 triangular islands and large area continuous films until now.

In this paper, we investigated and demonstrated the CVD growth of MoS_2 isolated triangular islands and large area continuous film by MoO_3 sulfurization in a home-built furnace set-up. By controlling the timing of sulfur vaporization and the target substrate position, the synthesis of these two types of MoS_2 was selectable and able to perform independently with different growth mechanisms. The CVD growth of MoS_2 isolated triangular islands was proceeded with a seed nucleation process, where the MoS_2 large area continuous film growth was dominated by a MoO_3 limited process. Hydrofluoric acid (HF) treatment for target substrates was also found to modulate the size and density of the MoS_2 triangular islands, by changing the substrate

Manuscript received September 18, 2015; revised January 13, 2016; accepted January 25, 2016. Date of publication February 3, 2016; date of current version March 8, 2016. This work was supported in part by an unrestricted Grant from SEMATECH (GMGS14EG02) and the Hong Kong Polytechnic University under Project G-UC72. The review of this paper was arranged by Associate Editor H. Zhang.

W. C. Cho, K. L. Wu, P. S. Yip, and K. M. Lau are with the Photonics Technology Center, Department of Electronic and Computer Engineering, Hong Kong University of Science and Technology, Kowloon, Hong Kong (e-mail: wccho@ust.hk; klwuaa@ust.hk; psyip@ust.hk; eekmlau@ust.hk).

X. Wang is with the CAS Key Laboratory of Standardization and Measurement for Nanotechnology, National Center for Nanoscience and Technology, Beijing 100190, China (e-mail: wangxsh2001@gmail.com).

Y. Chai is with the Department of Applied Physics, Hong Kong Polytechnic University, Kowloon, Hong Kong (e-mail: y.chai@polyu.edu.hk).

Color versions of one or more of the figures in this paper are available online at http://ieeexplore.ieee.org.

Digital Object Identifier 10.1109/TNANO.2016.2524044

surface condition. Raman spectroscopy, photoluminescence (PL) and atomic force microscopy (AFM) were used to characterize and compare the as-grown samples. The MoS_2 isolated triangular islands were monolayers with a grain size of up to $\sim$70 μm; where the continuous thin film was composed of coalesced and overlapped MoS_2 nanosheets, with a smooth surface morphology and large covered area of centimeters in size. Back gated FETs (W/L = 38/6 μm) of the as-grown samples were fabricated by O_2 plasma and reactive ion etching, photolithography and metallization. Without any dielectric engineering and post growth treatment, the devices showed high field effect mobilities of 11.42 cm^2/V.s and 4.04 cm^2/V.s for MoS_2 triangular islands and large area continuous films respectively. The devices also demonstrated a nearly ideal current saturation characteristic under a wide range of drain and gate biases and an excellent on/off current ratio over 10^8, which showed the real potential of CVD MoS_2 devices for future electronic applications.

II. Experimental Details

A. Substrate Treatment

P-type Si (100) was used as the starting substrate. A 300 nm SiO_2 layer was thermally grown on the Si substrates by wet oxidation. Prior to the MoS_2 growth, the substrates were cleaned with acetone, isopropanol (IPA), and deionized (DI) water in an ultrasonic bath. The substrates were then soaked in a HCl:HNO_3 (2:1) solution followed by a DI water rinse. For MoS_2 triangular islands growth, an additional HF (5%) dip was performed for the substrates followed by being blown dry.

B. MoS_2 Synthesis

The CVD MoS_2 growth was performed in a home-built dual-zone furnace system with a 25 mm horizontal quartz tube at atmospheric pressure. MoO_3 powder (Sigma Aldrich, 99.5%) and sulfur (Sigma Aldrich, 99.5%) were used as the precursor and reactant material, respectively. A small SiO_2/Si substrate was uniformly covered with MoO_3 powder and placed at the center of a quartz boat. The 1.5 cm $\times$ 2 cm SiO_2/Si target substrate was placed either on top of the MoO_3 powder or downstream in the furnace, depending on what type of MoS_2 was to be grown. The whole set-up was loaded into the center of the furnace after the 900 °C dummy baking for 30 minutes with 300 sccm ultrahigh purity argon (Ar) gas. Another quartz boat containing sulfur powder was placed at the upstream of and outside the furnace. The sulfur was heated independently by a heating pad wrapped around the boat during the CVD process.

For the MoS_2 triangular islands growth, the position of the target SiO_2/Si substrate was on the top of the MoO_3 powder. The furnace was heated up to 500 °C with a rate of 20 °C/min while flowing with 50 sccm Ar gas. After that, the furnace was further ramped up to 750 °C at a rate of 10 °C/min. The heating pad that wrapped the sulfur powder was immediately turned on when the furnace temperature just reached 750 °C. After holding at 750 °C for 10 minutes, the furnace temperature was increased to 900 °C at a heating rate of 5 °C/min and held at this for 20 minutes. Then the furnace was cooled down to 550 °C at 10 °C/min and the heating pad was removed from the sulfur powder. The furnace was then shut down and naturally cooled to room temperature.

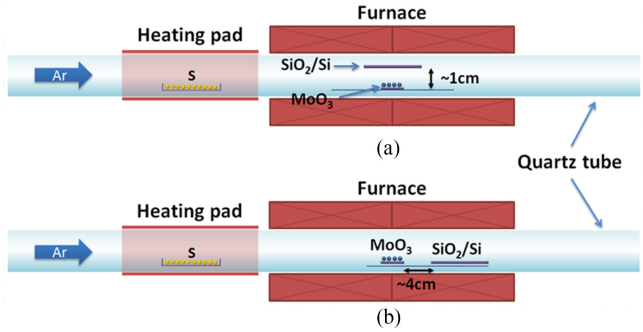

Fig. 1. CVD furnace set-up for the growth of MoS_2 (a) triangular islands and (b) large area continuous thin film.

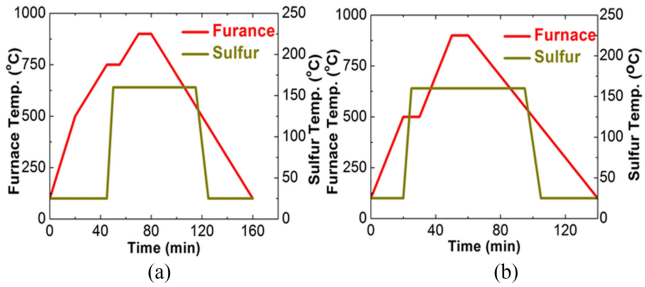

Fig. 2. Schematic illustration of typical growth of MoS_2 (a) triangular islands and (b) large area continuous thin film.

For synthesis of the MoS_2 continuous thin film, the target SiO_2/Si substrate was placed at the downstream in the furnace. The furnace temperature was increased to 500 °C at a heating rate of 20 °C/min while flowing with 50 sccm Ar gas. When the temperature just reached 500 °C, the heating pad was immediately switched on and the sulfur powder was left to sublimate. After holding the furnace temperature at 500 °C for 10 minutes, the furnace was further ramped up to 900 °C at a rate of 20 °C/min. After holding at 900 °C for 10 minutes, the furnace was cooled down to 550 °C and the heating pad was removed. Finally, the furnace was turned off and cooled to room temperature. Figs. 1. and 2. show the CVD system set-ups and the schematic illustrations of the MoS_2 growth.

C. Materials Characterization

The step height and surface morphologies of the samples were measured by atomic force microscopy (AFM). Raman spectroscopy was used to analyze the quality and thickness of MoS_2 crystals [21], [22]. Similar to graphene, Raman spectra of MoS_2 crystals were found to be layer dependent and the peak shift difference between the two major modes ($E^1{}_{2g}$ and A_{1g}) is able to estimate the number of layers. Photoluminescence (PL) was also done to characterize the optical properties of the samples. Both the Raman spectra and PL measurement were conducted with a confocal Raman microscope (Renishaw). The

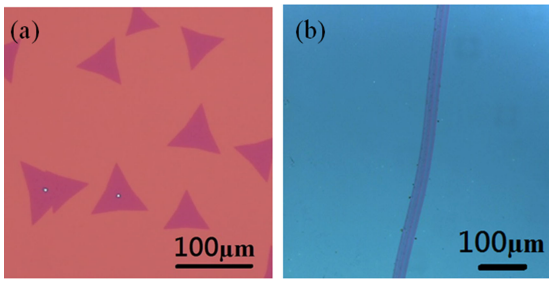

Fig. 3. Microscopic images of MoS_2 (a) isolated triangular islands and (b) large area continuous thin film with a scratched tweezer mark.

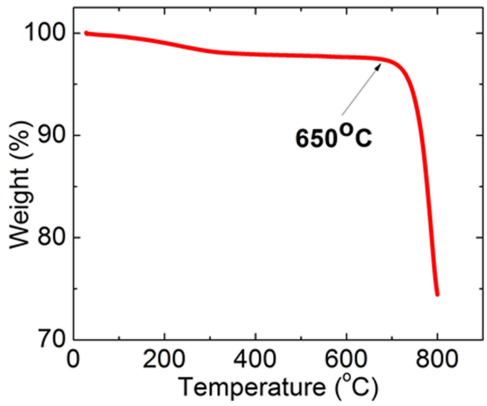

Fig. 4. Thermogravimetric curve with weight percentage versus ramping temperature of the MoO_3 powder

wavelength and power of the laser was 514.5 nm and 3 mW. Raman mapping was also conducted for the continuous thin film to analyze the uniformity.

D. Devices Fabrication and Characterization

Both the as-grown MoS_2 triangular islands and continuous thin film were used to fabricate back-gated FETs. Standard photolithography was used in the fabrication process. The FETs active regions were first defined with photoresist. For the MoS_2 triangular islands, the active regions were patterned with O_2 plasma. For the continuous thin film, CHF_3/O_2 reactive ion etching (RIE) was used to remove the film areas outside of the active regions. The film was over-etched by RIE forming rectangular mesas on the SiO_2 substrate. The source/drain (S/D) electrode regions of the FETs were patterned by a second photolithography step. After deposition of the contact metal Ti/Au (10/190 nm) by electron beam evaporation and the formation of the electrodes by a metal lift-off process, the back side thermal oxide was entirely removed by buffered oxide etchant (BOE). The devices were baked on a 110 °C hotplate to remove any solvents introduced during the fabrication process. DC electrical characteristics were characterized using an Agilent 4156C semiconductor parametric analyzer at room temperature under dark ambient conditions.

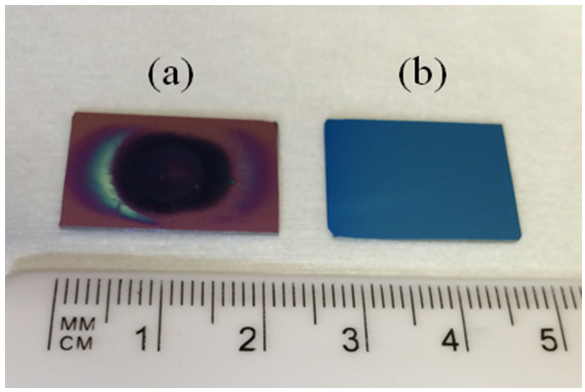

Fig. 5. Photo images of 1.5 cm × 2 cm MoS_2 (a) non-uniform continuous film formed by placing the target substrate just above of the MoO_3 source and (b) large area continuous thin film

III. Results and Discussion

A. Effect of Growth Parameters and Substrates Position on MoS_2 Crystallinity

In this report, we successfully demonstrated the selectable growth of MoS_2 with two kinds of crystallinity. Fig. 3 shows the microscopic images of MoS_2 samples. Typical highly crystalline isolated MoS_2 triangular islands were found in the middle region of the target substrate with a size of up to ~70 μm, which is shown in Fig. 3 (a). In Fig. 3 (b), a tweezer mark was used to generate an optical contrast between the MoS_2 continuous thin film and the SiO_2/Si substrate. The uniform and clean light blue MoS_2 thin film is continuous with an area of up to centimeters.

The selectable MoS_2 growth was mainly achieved by controlling the timing of the sulfur vaporization and the substrate's position. First of all, we performed a thermal gravimetric analysis (TGA) to characterize the sublimation properties of the MoO_3 powder. Fig. 4 shows the corresponding thermogravimetric curve. We found that the MoO_3 powder started vaporizing at ~650 °C and we defined this as the crucial point of temperature to differentiate between our MoS_2 triangular island and continuous thin film growth.

In the growth of MoS_2 triangular islands, the heating pad was turned on and the sulfur vaporized when the furnace ramped up to 750 °C. According to the TGA result, the MoO_3 powder had already sublimated before the sulfur vaporized and the tube ambient was filled with MoO_3 vapor. The furnace was then held at 750 °C for 10 mins. At the beginning, the MoO_3 partial pressure (P_{moo3}) was far higher than the sulfur partial pressure (P_s), which favored the incomplete reactions of MoO_3 and sulfur. Oxysulfide clusters were then created and nucleated on the target substrate [5], [23], [24], while the P_s kept increasing during the process and eventually became steady. Finally, the oxysulfide clusters were further reacted with sulfur vapor and MoS_2 triangular islands were formed. After that, the furnace was ramped up to 900 °C while maintaining a constant sulfur supply to ensure the complete sulfurization of oxysulfide clusters and improve the MoS_2 crystalline quality [16]. During the MoS_2 triangular islands synthesis, the MoO_3 incomplete sulfurization and oxysulfide sulfurization coexisted

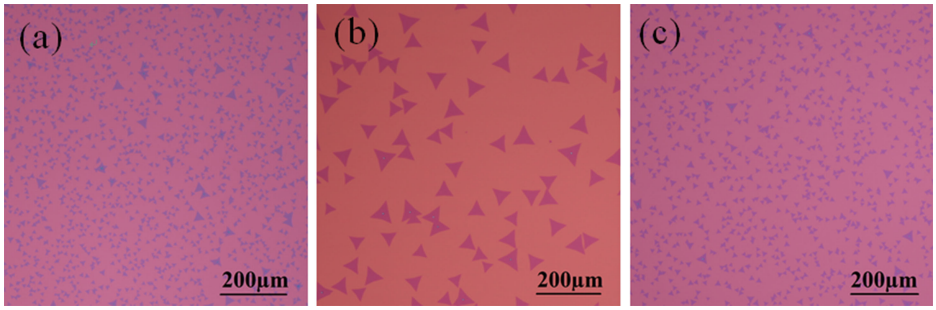

Fig. 6. Photo images of MoS_2 triangular islands samples (a) without HF substrate treatment, (b) after HF surface treatment and (c) DI rinse after HF surface treatment.

and competed with each other. This led the slow formation of MoS_2 vapor and the MoS_2 partial pressure (P_{mos2}) became relatively low. Based on the law of mass reaction, the low P_{mos2} resulted in slow MoS_2 deposition rate and the formation of highly crystalline MoS_2 triangular islands became favored [15].

In the growth of MoS_2 continuous thin film, heating up of the sulfur was started when the furnace temperature reached 500 °C. After that, the furnace was ramped up to 900 °C and to vaporize the MoO_3 powder. Since the tube was already full of sulfur vapor prior to the MoO_3 vaporization, the MoO_3 acted as the limited reactant and MoS_2 was formed immediately when the MoO_3 powder was just vaporized. The fast MoS_2 formation resulted in the rapid increase of its partial pressure. When the P_{mos2} increased to higher than its vapor pressure, MoS_2 started to deposit on the target substrate. According to the law of mass reaction, the rapid increase of MoS_2 vapor created a high P_{mos2} and led to a fast deposition rate, which favored the formation of small grain size MoS_2 thin film [15]. Similar to the growth of triangular islands, the furnace was eventually ramped up to 900 °C which aimed to improve the crystalline quality. Furthermore, we found that the placement of the target substrate would affect the uniformity of the MoS_2 film. We tried to place the target substrate on top of the MoO_3 which was similar to the triangular islands growth. Unfortunately a non-uniform MoS_2 film was formed which is shown in Fig. 5 (a). As the gradient of P_{moo3} was large at the furnace center [25], different thicknesses of MoS_2 would be easily formed and deposited on the target substrate. We then switched the target substrate position to the downstream of the furnace which was in series with the MoO_3 holder substrate. As the target substrate was put away from the MoO_3 source, the P_{mos2} became steady when the vapors reached the substrate due to mass transfer. This approach enhanced the uniform MoS_2 deposition and resulted in the formation of large area uniform MoS_2 continuous thin film, which is shown in Fig. 5 (b).

To summarize, the main difference between the CVD growth of MoS_2 triangular islands and continuous thin film was the timing control of the sulfur supply. For MoS_2 triangular islands, the MoO_3 was vaporized before the sulfur vaporization leading to the dominated seed nucleation process, while for MoS_2 continuous thin film, the MoO_3 vaporization proceeded after filling the tube with sulfur vapor, resulting in the dominated MoO_3 limited process.

B. Effect of HF Treatment on the Growth of MoS_2 Triangular Islands

Fig. 6 shows the microscopic images of the as-grown MoS_2 triangular islands samples with three different cleaning methods. Sample 1 was cleaned by acetone, IPA and HCl/HNO_3. Sample 2 was treated by an additional 5% HF dip for a few seconds; and for sample 3, an additional DI water rinse was performed after the HF dip. From Fig. 6, we observe that grain size and density of triangular islands differ among the samples, where sample 2 shows the largest grain sizes of $\sim$70 μm on average and the lowest grains density. During the HF dip of the SiO_2/Si substrates, some fluorine atoms bonded to the SiO_2 surface or even embedded in the oxide [26]–[28]. Partial negative charges were then created on the oxide surface due to the high electronegativity of the terminated fluorine atoms. Similar partial negative charges could also be found in the oxysulfide since its molecular structure was terminated either by electronegative oxygen or sulfur atoms [23]. Since both the oxysulfide and fluorinated oxide surface carried the same type of partial charges, the tendency of the oxysulfide nucleated on the target substrate decreased due to some degree of electrostatic repulsion. As a result, the reduction of nucleation sites caused the decrease in the MoS_2 triangular islands density. In addition, due to the decrease of nucleation sites, more sulfur was consumed on each site while keeping the P_s constant, resulting in the size increase of MoS_2 triangular islands [18].

Fig. 6 (c) shows the image of sample 3 which had been treated with a DI water rinse after the HF dip. We observe that the MoS_2 triangular islands returned to a similar size to sample 1. This is probably due to the F atoms on the oxide surface being substituted back to hydroxyl (OH) groups, leading to the reformation of the hydrophilic oxide surface. The approach provides a new way for MoS_2 grain size modulation. We believed that by further optimizing the growth recipe and integrating it with the HF surface treatment, the size of single crystal MoS_2 triangular islands can be further increased.

C. Surface Morphology and Optical Properties

Fig. 7 shows the 10 μm x 10 μm AFM images of the MoS_2 triangular islands and the continuous thin film respectively. For triangular islands, the number of layers can be estimated by the flake thickness. The thickness of MoS_2 triangular islands is determined to be $\sim$0.8 nm by scanning across the flake edge,

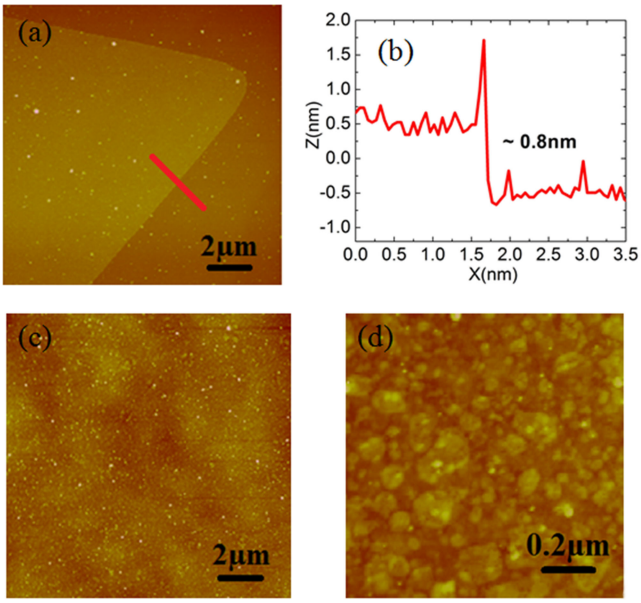

Fig. 7. 10 μm $\times$ 10 μm AFM image of the MoS_2 (a) triangular islands and (b) the height profile with the red scanning line. (c) 10 μm $\times$ 10 μm and (d) 1 μm $\times$ 1 μm AFM image of MoS_2 continuous thin film surface.

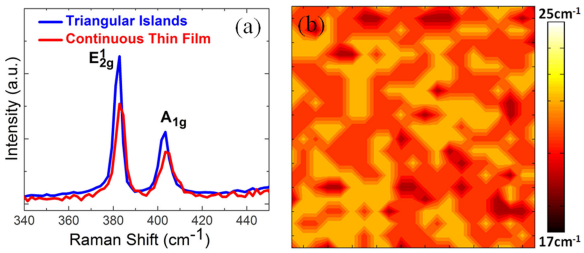

Fig. 8. (a) Raman spectra of the MoS_2 triangular islands and continuous thin film. (b) Raman mapping of the E^1_{2g} and A_{1g} peak spacing corresponding to the MoS_2 continuous thin film.

which is agreed to be a monolayer from the previous studies [1]–[3]. For MoS_2 continuous thin film, the thickness cannot be determined accurately due to the absence of natural film edges. Observation of the AFM image of the MoS_2 continuous thin film shows the continuous film is composed of MoS_2 nanosheets with very small grain size, which are on average smaller than 300 nm. The surface morphology is smooth with a measured root mean square (RMS) roughness of $\sim$0.6 nm. Fig. 7 (d) also shows the AFM image of the MoS_2 continuous thin film with a smaller scanning area of 1 μm $\times$ 1 μm.

Fig. 8 (a) shows the Raman spectra of the MoS_2 triangular islands (blue line) and the continuous thin film (red line). For MoS_2 triangular islands, the E^1_{2g} and A_{1g} modes locate at 382.8 cm^{-1} and 403.4 cm^{-1} respectively, with a peaks spacing of 20.6 cm^{-1}. The value corresponds to MoS_2 monolayer flakes according to previous studies [21], [22] and is consistent with the AFM results. Fig. 8 (b) shows the Raman mapping image of the peak difference between the E^1_{2g} and A_{1g} mode for MoS_2 continuous thin film over an area of 10 μm x 10 μm with the scanning steps of 0.5 μm. The peak spacing mainly

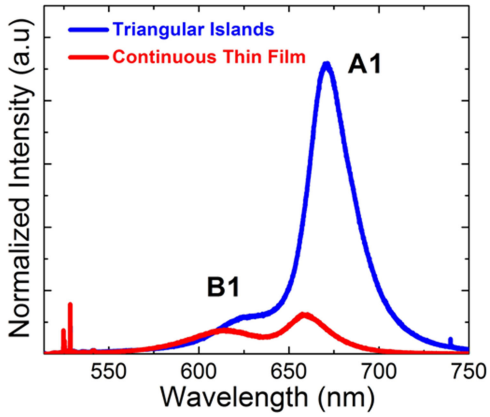

Fig. 9. PL spectrum of the MoS_2 triangular islands and continuous thin film. The A1exitation peak is derived from the direct band gap and the B1 peak come from the valence band splitting. The A1 peaks of MoS_2 triangular islands and continuous thin film are located at 672 nm and 658 nm respectively.

varied from 19.6 to 22.3 cm^{-1}. The signals of $\sim$20 cm^{-1} were coming from coalesced monolayer MoS_2 crystals. Where for the signals of $\sim$22 cm^{-1}, it was believed to be corresponding to a double layer MoS_2 or overlapped region of monolayer MoS_2 nanosheets. Since the grain sizes of the MoS_2 nanosheets are very small in nature ($<$ 300 nm) and the spot size of the Raman laser is 1 μm, the Raman spectra might be dominated by the high density overlapped regions at the MoS_2 monolayer boundaries, which might give out the misleading double layer signals. The representative Raman spectra of MoS_2 continuous thin film with the peak spacing of 22.3 cm^{-1} is plotted in Fig. 8 (a). The full width half maximum (FWHM) of the A_{1g} peak for MoS_2 triangular islands and continuous thin film are 4.1 cm^{-1} and 6.2 cm^{-1}, respectively, the 34% difference indicates the MoS_2 triangular islands had better quality.

The PL spectrums of the MoS_2 triangular islands (blue line) and the continuous thin film (red line) are shown in Fig. 9. The PL peaks were normalized to the intensity of the A_{1g} peak to screen out other external factors [29] and make a fair comparison of PL peaks' intensities. For MoS_2 triangular islands, a remarkably strong A1 excitation peak is observed and located at 672 nm (1.84 eV), which agrees with the direct band transition at the K point of the Brillouin zone [1], [2], [6], [29]– [31]. Where for the MoS_2 continuous thin film, a comparatively weaker peak from A1 excitons located at 658 nm (1.88eV). Similar to the Raman results, the double layer MoS_2 and overlapped regions of the MoS_2 nanosheets might contribute to the PL signals. The varied local doping and strain around the overlapped regions and grain boundaries of small grain size MoS_2 nanosheets might modulate the direct band structure, leading to the lowering intensity and blue shift 40 meV of the A1 peak [5], [32], [33].

D. Electrical Characterization

The as-grown MoS_2 triangular islands and continuous thin film were used to fabricate back-gated FETs to evaluate their electrical properties. Fig. 10 (a) shows the cross-sectional diagram of the MoS_2 FETs structure. In order to make a fair

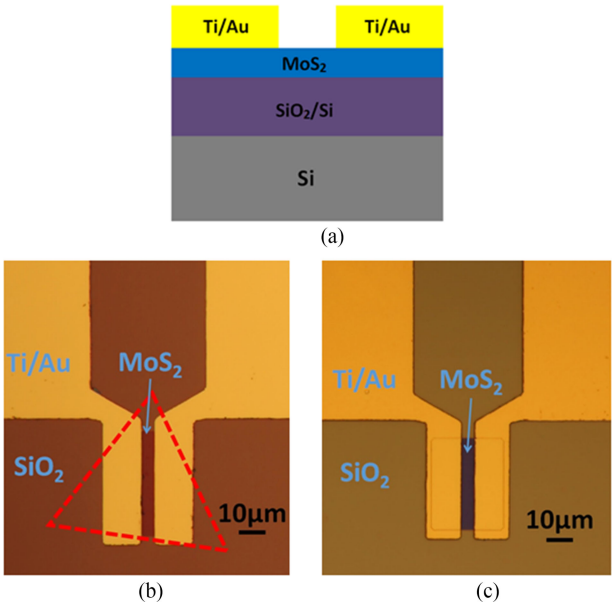

Fig. 10. (a) Device structure of the MoS_2 FETs. Aerial view of the MoS_2 (b) triangular islands, and (c) continuous thin film devices taken by optical microscope. The red dashed lines in (b) indicate the original position of the corresponding MoS_2 triangular island before the O_2 plasma patterning. The dimension of the FET is W/L = 38/6 μm.

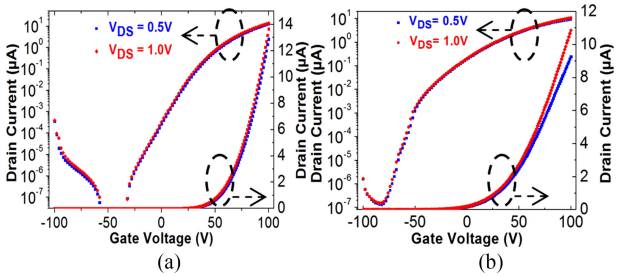

Fig. 11. Logarithmic scale and linear scale of transfer characteristics of the MoS_2 (a) triangular islands and (b) continuous thin film FETs.

comparison, both the triangular islands and continuous thin film devices were defined by the same drain/source spacing and the length of the MoS_2 active region (W/L = 38/6 μm). The source/drain (S/D) regions were completely covered with contact metals. Fig. 10 (b) and (c) show the optical images of typical MoS_2 triangular islands and continuous thin film FETs respectively. The blue MoS_2 regions are the channel materials of the FETs and the 300 nm thick thermal SiO_2 underneath acted as the gate dielectric. Gate bias was applied to the Si substrate to modulate the device.

Electrical measurements were conducted at room temperature and in a dark ambient setting. Fig. 11 shows the DC transfer characteristics (drain current vs. gate bias), in both logarithmic and linear scales of the MoS_2 FETs. The back gate voltage (V_{gs}) was swept from -100 V to $+100$ V, at two fixed drain voltages (V_{ds}) of $+0.5$ V and $+1.0$ V. Both the MoS_2 triangular islands and continuous thin film back-gated FETs were n-channel devices operating in the depletion mode. The devices could be turned

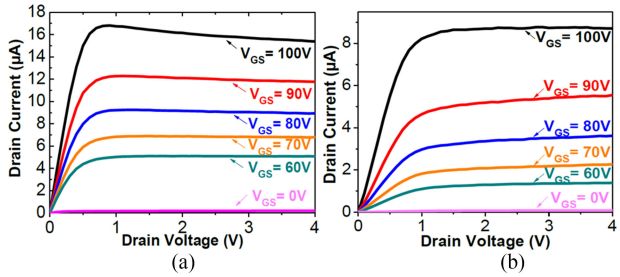

Fig. 12. Output curve of the of the MoS_2 (a) triangular islands and (b) continuous thin film FETs with several back gate voltage bias.

off nicely until large negative biases of $\sim$50 V and $\sim$75 V when the drain current started to increase slightly with a continuing decrease of the gate voltage, which might be attributed to the formation of p-type inversion channels with 2D holes gas [34], [35]. When biased in the positive direction, 2D electron gas accumulated in the conduction channel of the MoS_2 FETs. Furthermore, an on/off current ratio of up to and even over 10^8 for the MoS_2 devices had been obtained and this is one of the best values for CVD MoS_2 devices [5]–[19], [36]. The excellent on/off ratio is mainly attributed to the existence of the $\sim$ 1.9 eV band gap for both the MoS_2 triangular islands and continuous thin film. To estimate the field effect mobility of the MoS_2 FETs, the measured differential resistance was used [3]: $\mu = (\Delta I_{ds}/\Delta V_g) \times (L/WC_{ox}V_{ds})$, where C_{ox} is the gate capacitance per unit area, L is the channel length, W is the channel width and $\Delta I_{ds}/\Delta V_g$ is the slope of the transfer curve taken in the linear region. With $C_{ox} = 1.15 \times 10^{-4}$ F.m^{-2} for 300 nm thick thermal oxide and L/W = 6/38 μm, the calculated field effect mobilities of the as-grown MoS_2 triangular islands and continuous thin film FETs were 11.42 cm^2/V.s and 4.04 cm^2/V.s at $V_{ds} = 0.5$ V respectively, which showed the high quality of the MoS_2 devices compared with recent studies [5]–[19], [36]. Contact resistance had not been extracted and included in the calculation, which may have resulted in an underestimate of mobilities. The result was also consistent with the Raman and PL measurements, showing that the single crystal MoS_2 triangular islands have better quality than the continuous thin film, leading to the higher electron mobility. From Fig. 11 (a) and (b), due to worse gate control through the bulk Si/SiO_2 gate dielectric, the estimated subthreshold swings (SS) suffered from a large value of $\sim$9 V/dec and $\sim$6 V/dec, compared to those of back-gated [35], [37] or top-gated devices [3], [38], respectively, with high-k materials as the gate dielectric. The output characteristics of the MoS_2 FETs in Fig. 12 were measured by sweeping the V_{ds} from 0 V to $+4$ V, with gate modulation steps of -10 V. Note that both the MoS_2 triangular islands and continuous thin film devices exhibited near ideal current saturation characteristics over a large V_{ds} range under various V_{gs} biases, whereas most reported devices made with 2D materials show less ideal current saturation characteristics. For $V_{gs} = +100$ V, the drain current starts to saturate with V_{ds} of $\sim$1 V with on-state current of $\sim$16 μA and $\sim$9 μA. A transistor with near ideal current saturation is important for its implementation in many circuit applications such as current

mirrors. Most recently, a CVD MoS_2 triangular island FET has been demonstrated with a clear current saturation effect under a high V_{ds} bias [36]. However, the reasons behind the phenomenon and the complete mechanism in these MoS_2 FETs still need to be further investigated theoretically and experimentally in the future.

IV. Conclusion

In summary, we demonstrated the selectable growth of 2D MoS_2 with different crystallinity by simply controlling the sulfur vaporization timing and target substrate positions. The growth of MoS_2 triangular islands is a seed nucleation process, where the MoS_2 continuous thin film growth is a MoO_3 limited process. AFM, Raman and PL measurements were used to characterize the samples. The MoS_2 isolated triangular islands are monolayers and highly crystalline in nature, where the large area continuous thin film is composed of small grain size MoS_2 nanosheets with a covered area of up to centimeters. HF surface treatment has also been demonstrated to modulate the grain density and enlarge the grain sizes of MoS_2 triangular islands. The fabricated back-gated FETs were measured with high mobilities of 11.42 cm^2/V.s and 4.04 cm^2/V.s for MoS_2 triangular islands and continuous thin film respectively, with an excellent current on/off ratio up to over 10^8. The FETs also showed an uncommon current saturation phenomenon within 2D devices, which demonstrated the real potential of future low power electronic devices.

Acknowledgment

The authors would like to thank C. W. Tang, X. Zou, W. C. Chong, X. Lu, and H. Jiang for many useful discussions.

References

[1] K. F. Mak, C. Lee, J. Hone, J. Shan, and T. F. Heinz, "Atomically thin MoS_2: A new direct-gap MoS_2 semiconductor," *Phys. Rev. Lett.*, vol. 105, no. 12, p. 138605, Sep. 2010.

[2] Q. H. Wang, K. Kalantar-Zadehm, A. Kis, J. N. Coleman, and M. S. Strano, "Electronics and optoelectronics of two-dimensional transition metal dichalcogenides," *Nature Nanotechnol.*, vol. 7, pp. 699–712, Nov. 2012.

[3] B. Radisavljevic, A. Radenovic, J. Brivio, V. Giacometti, and A. Kis, "Single-layer MoS_2 transistors," *Nature Nanotechnol.*, vol. 6, pp. 147–150, Mar. 2011.

[4] D. Lembke and A. Kis, "Breakdown of high-performance monolayer MoS_2 transistors," *ACS Nano*, vol. 6, no. 11, pp. 10070–10075, Oct. 2012.

[5] S. Najmaei, Z. Liu, W. Zhou, X. Zou, G. Shi, S. Lei, B.I. Yakobson, J.-C. Idrobo, P.M. Ajayan, and J. Lou "Vapour phase growth and grain boundary structure of molybdenum disulphide atomic layers," *Nature Mater.*, vol. 12, pp. 754–759, Jun. 2013.

[6] Y. H. Lee, X. Q. Zhang, W. Zhang, M. T. Chang, C. T. Lin, K. D. Chang, Y. C. Yu, T. W. Wang, C. S. Chang, L. J. Li, and T. W. Lin, "Synthesis of large-area MoS_2 atomic layers with chemical vapor deposition," *Adv. Mater.*, vol. 24, pp. 2320–2325, Mar. 2012.

[7] W. Wu, D. De, S. C. Chang, Y. Wang, H. Peng, J. Bao, and S. S. Pei, "High mobility and high on/off ration field-effect transistors based on chemical vapor deposited single-crystal MoS_2 grains," *Appl. Phys. Lett.*, vol. 102, p. 142106, Apr. 2013.

[8] M. Amani, M. L. Chin,, A. G. Birdwell, T. P. O'Regan, S. Najmaei, Z. Liu, P.M. Ajayan, J. Lou, and M Dubey, "Electrical performance of monolayer MoS_2 field-effect transistors prepared by chemical vapor deposition," *Appl. Phys. Lett.*, vol. 102, p. 193107, May 2013.

[9] M. Amani, M.L. Chin, A.L. Mazzoni, R.A. Burke, S. Najmaei, P.M. Ajayan, J. Lou, and M. Dubey, "Growth-substrate induced performance degradation in chemically synthesized monolayer MoS2 field effect transistors," *Appl. Phys. Lett.*, vol. 104, p. 203506, May 2014.

[10] H. Schmidt, S. Wang, L. Chu, M. Toh, R. Kumar, W. Zhao, A. H. Castro Neto, J. Martin, S. Adam, B. Özyilmaz, G. Eda, "Transport properties of monolayer MoS_2 grown by chemical vapor deposition," *Nano Lett.*, vol. 14, pp. 1909–1913, Mar. 2014.

[11] H. Liu, M. Si, S. Najmeai, A. T. Neal, Y. Du, P. M. Ajayan, J. Lou, and P. D. Ye, "Dual-gate MOSFETs on monolayer CVD MoS_2 films," in *Proc. IEEE Device Res. Conf.*, Jun. 2013, pp. 163–164.

[12] Y. Zhan, Z. Liu, S. Najmaei, P. M. Ajayan, and J. Lou. "Large-area vapor-phase growth and characterization of MoS_2 atomic layers on a SiO_2 substrate," *Small*, vol. 8, pp. 966–971, Apr. 2012.

[13] X. Wang, H. Feng, Y. Wu, and L. Jiao, "Controlled synthesis of highly crystalline MoS_2 flakes by chemical vapor deposition," *J. Amer. Chem. Soc.*, vol. 135, pp. 5304–5307, Apr. 10, 2013.

[14] M. R. Laskar, L. Ma, S. Kannappan, P. S. Park, S. Krishnamorrthy, D. N. Nath, W. Lu, Y. Wu, and S. Rajan, "Large area single crystal (0001) oriented MoS_2," *Appl. Phys. Lett.*, vol. 102, p. 252108, June. 2013.

[15] Y. Yu, C. Li, Y. Liu, L. Su, Y. Zhang, and L. Cao, "Controlled scalable synthesis of uniform, high-quality monolayer and few layer MoS_2 films," *Sci. Rep.*, vol. 3, p. 1866, May 2013.

[16] Y. Lee, J. Lee, H. Bark, I. K. Oh, G. H. Ryu, Z. Lee, H. Kim, J. H. Cho, J. H. Ahn, and C. Lee, "Synthesis of wafer-scale uniform molybdenum disulfide films with control over the layer number using a gas phase sulfur precursor," *Nanoscale*, vol. 6, pp. 2821–2826, Dec 2013.

[17] J. Zhang, H. Yu, W. Chen, X. Tian, D. Liu, M. Cheng, G. Xie, W. Yang, R. Yang, X. Bai, D. Shi, and G. Zhang, "Scalable growth of high-quality polycrystalline MoS_2 monolayers on SiO_2 with tunable grain sizes," *ACS Nano*, vol. 8, no. 6, pp. 6024–6030, May 2014.

[18] J. Jeon, S. K. Jang, S. M. Jeon, G. Yoo, J. H. Park, and S. Lee, "Controlling grain size and continuous layer growth in two-dimensional MoS_2 films for nanoelectronic device application," *IEEE Trans. Nanotechnol.*, vol. 14, no. 2, pp. 238–242, Dec. 2014.

[19] Y. C. Lin, W. Zhang, J. K. Huang, K. K. Liu, Y. H. Lee, C. T. Liang, C. W. Chu, and L. J. Li, "Wafer-scale MoS_2 thin layers prepared by MoO_3 sulfurization," *Nanoscale*, vol. 4, pp. 6636–6641, Aug. 2012.

[20] Z. Lin, Y. Zhao, C. Zhou, R. Zhong, X. Wang, Y. H. Tsang, and Y. Chai, "Controllable growth of large–size crystalline MoS_2 and resist-free transfer assisted with a cu thin film," *Sci. Rep.*, vol. 5, p. 18596, Dec. 2015.

[21] C. Lee, H. Yan, L. E. Brus, T. F. Heinz, J. Hone, and S. Ryu, "Anomalous lattice vibrations of single- and few-layer MoS_2," *ACS Nano*, vol. 4, no. 5, pp. 2695–2700, Apr. 2010.

[22] H. Li, Q. Zhang, C. C. R. Yap, B. K. Tay, T. H. Tong, A. Oliver and D. Bailargeat, "From bulk to monolayer MoS_2: Evolution of Raman scattering," *Adv. Func. Mater*, vol. 22, pp. 1385–1390, Jan 2012.

[23] T. H. Weber, J. C. Muijsers, J. H. M. C. Van Wolput, C. P. J. Verhagen, and J. W. Niemantsverdriet, "Basic reaction steps in the sulfidation of crystalline MoO_3 to MoS_2, as studied by X-ray photoelectron and infrared emission spectroscopy," *J. Phys. Chem.*, vol. 100, pp. 14144–14150, Aug. 1996.

[24] R. Ionescu, W. Wang, Y. Chai, Z. Mutlu, I. Ruiz, Z. Favors, D. Wickramaratne, M. Neupane, L. Zavala, R. Lake, M. Ozkan, and C.S. Ozkan, "Synthesis of automically thin MoS_2 triangles and hexagrams and their electrical transport properties," *IEEE Trans. Nanotechnol.*, vol. 13, no. 4, pp. 749–754, Apr. 2014.

[25] S. Wang, Y. Rong, Y. Fan, M. Pacios, H. Bhaskaran, K. He, and J-H. Warner, "Shape evolution of monolayer MoS_2 crystals grown by chemical vapor deposition," *Chem. Mater.*, vol. 26, pp. 6371–6379, Nov. 2014.

[26] K. Ljungberg, A. Söderbärg, and U. Jansson, "Improved direct bonding of Si and SiO_2 surfaces by cleaning in H_2SO_4: H_2O_2: HF," *Appl. Phy. Lett.*, vol. 67, pp. 650–652, May 1995.

[27] D. Martin Knotter, "Etching mechanism of vitreous silicon dioxide in HF-based solutions," *J. Amer. Chem. Soc.*, vol. 12, pp. 4345–4351, Apr. 2000.

[28] J. K. Kang and C. B. Musgrave, "The mechanism of HF/H_2O chemical etching of SiO_2," *J. Chem. Phys.*, vol. 116, pp. 275–280, Jan. 2002.

[29] A. Splendiani, L. Sun, Y. Zhang, T. Li, J. Kim, C. Y. Chim, G. Gali, and F. Wang, "Emerging photoluminescence in monolayer MoS_2," *Nano. Lett.*, vol. 10, pp. 1271–1275, Mar. 2010.

[30] G. Eda, H. Yamaguchi, D. Voiry, T. Fujita, M. Chen, and M. Chhowalla, "Photoluminescence from chemically exfoilated MoS_2," *Nano. Lett.*, vol. 11, pp. 5111–5116, Mar. 2011.

[31] K. F. Mak, K. He, C. Lee, G. H. Lee, J. Hone, T. F. Heinz, and J. Shan, "Tightly bound trions in monolayer MoS_2," *Nature Mater.*, vol. 12, pp. 207–211, Mar. 2013.

[32] H. J. Conley, B. Wang, J. I. Ziegler, R. F. Haglund Jr., S. T. Pantelides, and K. I. Bolotin, "Bandgap engineering of strained monolayer and bilayer MoS_2," *Nano. Lett.*, vol. 13, pp. 3626–3630, Jul. 2013.

[33] E. Scalise, M. Houssa, G. Pourtois, V. Afanas'ev, and A. Stesmans, "Strain-induced semiconductor to metal transition in the two-dimensional honeycomb structure of MoS_2," *Nano Res.*, vol. 5, no. 1, pp. 43–48, Nov. 2011.

[34] E. S. Kim, S. Kim, Y. S. Lee, S. Y. Lee, S. Lee, W. Choi, H. Peelaers, C. G. Van de Walle, W. S. Hwang, T. Kosel, and D. Jena, "Multilayer transition-metal dichalcogenide channel thin-film transistors," in *Proc. IEEE Int. Electron Devices Meeting*, Dec. 2012, pp. 108–111.

[35] S. Kim, A. Konar, W. S. Hwang, J. H. Lee, J. Lee, J. Yang, C. Jung, H. Kim, J. B. Yoo, J. Y. Choi, Y. W. Jin, S. Y. Lee, D. Jena, W. Choi, and K. Kim, "High-mobility and low-power thin-film transistors based on multilayer MoS_2 crystals," *Nature Commun.*, vol. 3, p. 1011, Aug. 2012.

[36] G. He, K. Ghosh, U. Singistti, H. Ramamoorthy, R. Somphonsane, G. Bohra, M. Matsunaga, A. Higuchi, N. Aoki, S. Najmaei, Y. Gong, X. Zhang, R. Vajtai, P. M. Ajayan, and J. P. Bird, "Conduction mechanisms in CVD-grown monolayer MoS_2 transistors: From variable-range hopping to velocity saturation," *Nano. Lett.*, vol. 15, no. 8, pp. 5052–5058, Jun. 2015.

[37] C. Zhou, X. Wang, S. Raju, Z. Lin, D. Villaroman, B. Huang, H. L. W. Chan, M. Chan, and Y. Chai, "Low voltage and high ON/OFF ratio field-effect transistors based on CVD MoS_2 and ultra high-k gate dielectric PZT," *Nanoscale*, vol. 7, pp. 8695–8700, Apr. 2015.

[38] H. Liu and P. D. Ye, "MoS_2 dual-gate MOSFET with atomic-layer-deposited Al_2O_3 as top-gate dielectric," *IEEE Electron Device Lett.*, vol. 33, no. 4, pp. 546–548, Apr. 2012.

Authors' biographies not available at the time of publication.